Fermi National Accelerator Laboratory

FERMILAB-Pub-99/043-E
CDF

A Measurement of b Quark Fragmentation Fractions in the Production of Strange and Light B Mesons in $p\bar{p}$ Collisions at $\sqrt{s}$ = 1.8 TeV

F. Abe et al.
The CDF Collaboration

Fermi National Accelerator Laboratory
P.O. Box 500, Batavia, Illinois 60510

April 1999

Submitted to *Physical Review D*

Operated by Universities Research Association Inc. under Contract No. DE-AC02-76CH03000 with the United States Department of Energy

Disclaimer

Distribution

Copyright Notification

FERMILAB-PUB-99/043-E

A measurement of b quark fragmentation fractions in the production of strange and light B mesons in $p\bar{p}$ collisions at $\sqrt{s} = 1.8$ TeV.

F. Abe,[17] H. Akimoto,[39] A. Akopian,[31] M. G. Albrow,[7] S. R. Amendolia,[27] D. Amidei,[20] J. Antos,[33] S. Aota,[37] G. Apollinari,[31] T. Arisawa,[39] T. Asakawa,[37] W. Ashmanskas,[5] M. Atac,[7] P. Azzi-Bacchetta,[25] N. Bacchetta,[25] S. Bagdasarov,[31] M. W. Bailey,[22] P. de Barbaro,[30] A. Barbaro-Galtieri,[18] V. E. Barnes,[29] B. A. Barnett,[15] M. Barone,[9] G. Bauer,[19] T. Baumann,[11] F. Bedeschi,[27] S. Behrends,[3] S. Belforte,[27] G. Bellettini,[27] J. Bellinger,[40] D. Benjamin,[6] J. Bensinger,[3] A. Beretvas,[7] J. P. Berge,[7] J. Berryhill,[5] S. Bertolucci,[9] S. Bettelli,[27] B. Bevensee,[26] A. Bhatti,[31] K. Biery,[7] C. Bigongiari,[27] M. Binkley,[7] D. Bisello,[25] R. E. Blair,[1] C. Blocker,[3] K. Bloom,[20] S. Blusk,[30] A. Bodek,[30] W. Bokhari,[26] G. Bolla,[29] Y. Bonushkin,[4] D. Bortoletto,[29] J. Boudreau,[28] A. Brandl,[22] L. Breccia,[2] C. Bromberg,[21] N. Bruner,[22] R. Brunetti,[2] E. Buckley-Geer,[7] H. S. Budd,[30] K. Burkett,[11] G. Busetto,[25] A. Byon-Wagner,[7] K. L. Byrum,[1] M. Campbell,[20] A. Caner,[27] W. Carithers,[18] D. Carlsmith,[40] J. Cassada,[30] A. Castro,[25] D. Cauz,[36] A. Cerri,[27] P. S. Chang,[33] P. T. Chang,[33] H. Y. Chao,[33] J. Chapman,[20] M. -T. Cheng,[33] M. Chertok,[34] G. Chiarelli,[27] C. N. Chiou,[33] F. Chlebana,[7] L. Christofek,[13] M. L. Chu,[33] S. Cihangir,[7] A. G. Clark,[10] M. Cobal,[27] E. Cocca,[27] M. Contreras,[5] J. Conway,[32] J. Cooper,[7] M. Cordelli,[9] D. Costanzo,[27] C. Couyoumtzelis,[10] D. Cronin-Hennessy,[6] R. Cropp,[14] R. Culbertson,[5] D. Dagenhart,[38] T. Daniels,[19] F. DeJongh,[7] S. Dell'Agnello,[9] M. Dell'Orso,[27] R. Demina,[7] L. Demortier,[31] M. Deninno,[2] P. F. Derwent,[7] T. Devlin,[32] J. R. Dittmann,[6] S. Donati,[27] J. Done,[34] T. Dorigo,[25] N. Eddy,[13] K. Einsweiler,[18] J. E. Elias,[7] R. Ely,[18] E. Engels, Jr.,[28] W. Erdmann,[7] D. Errede,[13] S. Errede,[13] Q. Fan,[30] R. G. Feild,[41] Z. Feng,[15] C. Ferretti,[27] I. Fiori,[2] B. Flaugher,[7] G. W. Foster,[7]

M. Franklin,[11] J. Freeman,[7] J. Friedman,[19] Y. Fukui,[17] S. Gadomski,[14] S. Galeotti,[27] M. Gallinaro,[26] O. Ganel,[35] M. Garcia-Sciveres,[18] A. F. Garfinkel,[29] C. Gay,[41] S. Geer,[7] D. W. Gerdes,[20] P. Giannetti,[27] N. Giokaris,[31] P. Giromini,[9] G. Giusti,[27] M. Gold,[22] A. Gordon,[11] A. T. Goshaw,[6] Y. Gotra,[28] K. Goulianos,[31] H. Grassmann,[36] C. Green,[29] L. Groer,[32] C. Grosso-Pilcher,[5] G. Guillian,[20] J. Guimaraes da Costa,[15] R. S. Guo,[33] C. Haber,[18] E. Hafen,[19] S. R. Hahn,[7] R. Hamilton,[11] T. Handa,[12] R. Handler,[40] W. Hao,[35] F. Happacher,[9] K. Hara,[37] A. D. Hardman,[29] R. M. Harris,[7] F. Hartmann,[16] J. Hauser,[4] E. Hayashi,[37] J. Heinrich,[26] A. Heiss,[16] B. Hinrichsen,[14] K. D. Hoffman,[29] C. Holck,[26] R. Hollebeek,[26] L. Holloway,[13] Z. Huang,[20] B. T. Huffman,[28] R. Hughes,[23] J. Huston,[21] J. Huth,[11] H. Ikeda,[37] M. Incagli,[27] J. Incandela,[7] G. Introzzi,[27] J. Iwai,[39] Y. Iwata,[12] E. James,[20] H. Jensen,[7] U. Joshi,[7] E. Kajfasz,[25] H. Kambara,[10] T. Kamon,[34] T. Kaneko,[37] K. Karr,[38] H. Kasha,[41] Y. Kato,[24] T. A. Keaffaber,[29] K. Kelley,[19] M. Kelly,[20] R. D. Kennedy,[7] R. Kephart,[7] D. Kestenbaum,[11] D. Khazins,[6] T. Kikuchi,[37] M. Kirk,[3] B. J. Kim,[27] H. S. Kim,[14] S. H. Kim,[37] Y. K. Kim,[18] L. Kirsch,[3] S. Klimenko,[8] D. Knoblauch,[16] P. Koehn,[23] A. Köngeter,[16] K. Kondo,[37] J. Konigsberg,[8] K. Kordas,[14] A. Korytov,[8] E. Kovacs,[1] W. Kowald,[6] J. Kroll,[26] M. Kruse,[30] S. E. Kuhlmann,[1] E. Kuns,[32] K. Kurino,[12] T. Kuwabara,[37] A. T. Laasanen,[29] S. Lami,[27] S. Lammel,[7] J. I. Lamoureux,[3] M. Lancaster,[18] M. Lanzoni,[27] G. Latino,[27] T. LeCompte,[1] S. Leone,[27] J. D. Lewis,[7] M. Lindgren,[4] T. M. Liss,[13] J. B. Liu,[30] Y. C. Liu,[33] N. Lockyer,[26] O. Long,[26] M. Loreti,[25] D. Lucchesi,[27] P. Lukens,[7] S. Lusin,[40] J. Lys,[18] K. Maeshima,[7] P. Maksimovic,[11] M. Mangano,[27] M. Mariotti,[25] J. P. Marriner,[7] G. Martignon,[25] A. Martin,[41] J. A. J. Matthews,[22] P. Mazzanti,[2] K. McFarland,[30] P. McIntyre,[34] P. Melese,[31] M. Menguzzato,[25] A. Menzione,[27] E. Meschi,[27] S. Metzler,[26] C. Miao,[20] T. Miao,[7] G. Michail,[11] R. Miller,[21] H. Minato,[37] S. Miscetti,[9] M. Mishina,[17] S. Miyashita,[37] N. Moggi,[27] E. Moore,[22] Y. Morita,[17] A. Mukherjee,[7] T. Muller,[16] A. Munar,[27] P. Murat,[27] S. Murgia,[21] M. Musy,[36] H. Nakada,[37] T. Nakaya,[5] I. Nakano,[12] C. Nelson,[7] D. Neuberger,[16] C. Newman-Holmes,[7] C.-Y. P. Ngan,[19] H. Niu,[3] L. Nodulman,[1] A. Nomerotski,[8] S. H. Oh,[6] T. Ohmoto,[12] T. Ohsugi,[12] R. Oishi,[37]

M. Okabe,[37] T. Okusawa,[24] J. Olsen,[40] C. Pagliarone,[27] R. Paoletti,[27] V. Papadimitriou,[35] S. P. Pappas,[41] N. Parashar,[27] A. Parri,[9] D. Partos,[3] J. Patrick,[7] G. Pauletta,[36] M. Paulini,[18] A. Perazzo,[27] L. Pescara,[25] M. D. Peters,[18] T. J. Phillips,[6] G. Piacentino,[27] M. Pillai,[30] K. T. Pitts,[7] R. Plunkett,[7] A. Pompos,[29] L. Pondrom,[40] J. Proudfoot,[1] F. Ptohos,[11] G. Punzi,[27] K. Ragan,[14] D. Reher,[18] A. Ribon,[25] F. Rimondi,[2] L. Ristori,[27] W. J. Robertson,[6] A. Robinson,[14] T. Rodrigo,[27] S. Rolli,[38] L. Rosenson,[19] R. Roser,[7] T. Saab,[14] W. K. Sakumoto,[30] D. Saltzberg,[4] A. Sansoni,[9] L. Santi,[36] H. Sato,[37] P. Schlabach,[7] E. E. Schmidt,[7] M. P. Schmidt,[41] A. Scott,[4] A. Scribano,[27] S. Segler,[7] S. Seidel,[22] Y. Seiya,[37] F. Semeria,[2] T. Shah,[19] M. D. Shapiro,[18] N. M. Shaw,[29] P. F. Shepard,[28] T. Shibayama,[37] M. Shimojima,[37] M. Shochet,[5] J. Siegrist,[18] A. Sill,[35] P. Sinervo,[14] P. Singh,[13] K. Sliwa,[38] C. Smith,[15] F. D. Snider,[7] J. Spalding,[7] T. Speer,[10] P. Sphicas,[19] F. Spinella,[27] M. Spiropulu,[11] L. Spiegel,[7] L. Stanco,[25] J. Steele,[40] A. Stefanini,[27] R. Ströhmer,[7a] J. Strologas,[13] F. Strumia, [10] D. Stuart,[7] K. Sumorok,[19] J. Suzuki,[37] T. Suzuki,[37] T. Takahashi,[24] T. Takano,[24] R. Takashima,[12] K. Takikawa,[37] M. Tanaka,[37] B. Tannenbaum,[4] F. Tartarelli,[27] W. Taylor,[14] M. Tecchio,[20] P. K. Teng,[33] Y. Teramoto,[24] K. Terashi,[37] S. Tether,[19] D. Theriot,[7] T. L. Thomas,[22] R. Thurman-Keup,[1] M. Timko,[38] P. Tipton,[30] A. Titov,[31] S. Tkaczyk,[7] D. Toback,[5] K. Tollefson,[30] A. Tollestrup,[7] H. Toyoda,[24] W. Trischuk,[14] J. F. de Troconiz,[11] S. Truitt,[20] J. Tseng,[19] N. Turini,[27] T. Uchida,[37] F. Ukegawa,[26] J. Valls,[32] S. C. van den Brink,[15] S. Vejcik III,[7] G. Velev,[27] R. Vidal,[7] R. Vilar,[7a] I. Vologouev,[18] D. Vucinic,[19] R. G. Wagner,[1] R. L. Wagner,[7] J. Wahl,[5] N. B. Wallace,[27] A. M. Walsh,[32] C. Wang,[6] C. H. Wang,[33] M. J. Wang,[33] A. Warburton,[14] T. Watanabe,[37] T. Watts,[32] R. Webb,[34] C. Wei,[6] H. Wenzel,[16] W. C. Wester III,[7] A. B. Wicklund,[1] E. Wicklund,[7] R. Wilkinson,[26] H. H. Williams,[26] P. Wilson,[7] B. L. Winer,[23] D. Winn,[20] D. Wolinski,[20] J. Wolinski,[21] S. Worm,[22] X. Wu,[10] J. Wyss,[27] A. Yagil,[7] W. Yao,[18] K. Yasuoka,[37] G. P. Yeh,[7] P. Yeh,[33] J. Yoh,[7] C. Yosef,[21] T. Yoshida,[24] I. Yu,[7] A. Zanetti,[36] F. Zetti,[27] and S. Zucchelli[2]

(CDF Collaboration)

[1] *Argonne National Laboratory, Argonne, Illinois 60439*

[2] *Istituto Nazionale di Fisica Nucleare, University of Bologna, I-40127 Bologna, Italy*

[3] *Brandeis University, Waltham, Massachusetts 02254*

[4] *University of California at Los Angeles, Los Angeles, California 90024*

[5] *University of Chicago, Chicago, Illinois 60637*

[6] *Duke University, Durham, North Carolina 27708*

[7] *Fermi National Accelerator Laboratory, Batavia, Illinois 60510*

[8] *University of Florida, Gainesville, Florida 32611*

[9] *Laboratori Nazionali di Frascati, Istituto Nazionale di Fisica Nucleare, I-00044 Frascati, Italy*

[10] *University of Geneva, CH-1211 Geneva 4, Switzerland*

[11] *Harvard University, Cambridge, Massachusetts 02138*

[12] *Hiroshima University, Higashi-Hiroshima 724, Japan*

[13] *University of Illinois, Urbana, Illinois 61801*

[14] *Institute of Particle Physics, McGill University, Montreal H3A 2T8, and University of Toronto, Toronto M5S 1A7, Canada*

[15] *The Johns Hopkins University, Baltimore, Maryland 21218*

[16] *Institut für Experimentelle Kernphysik, Universität Karlsruhe, 76128 Karlsruhe, Germany*

[17] *National Laboratory for High Energy Physics (KEK), Tsukuba, Ibaraki 305, Japan*

[18] *Ernest Orlando Lawrence Berkeley National Laboratory, Berkeley, California 94720*

[19] *Massachusetts Institute of Technology, Cambridge, Massachusetts 02139*

[20] *University of Michigan, Ann Arbor, Michigan 48109*

[21] *Michigan State University, East Lansing, Michigan 48824*

[22] *University of New Mexico, Albuquerque, New Mexico 87131*

[23] *The Ohio State University, Columbus, Ohio 43210*

[24] *Osaka City University, Osaka 588, Japan*

[25] *Universita di Padova, Istituto Nazionale di Fisica Nucleare, Sezione di Padova, I-35131 Padova, Italy*

[26] *University of Pennsylvania, Philadelphia, Pennsylvania 19104*

[27] *Istituto Nazionale di Fisica Nucleare, University and Scuola Normale Superiore of Pisa, I-56100 Pisa, Italy*

[28] *University of Pittsburgh, Pittsburgh, Pennsylvania 15260*

[29] *Purdue University, West Lafayette, Indiana 47907*

[30] *University of Rochester, Rochester, New York 14627*

[31] *Rockefeller University, New York, New York 10021*

[32] *Rutgers University, Piscataway, New Jersey 08855*

[33] *Academia Sinica, Taipei, Taiwan 11530, Republic of China*

[34] *Texas A&M University, College Station, Texas 77843*

[35] *Texas Tech University, Lubbock, Texas 79409*

[36] *Istituto Nazionale di Fisica Nucleare, University of Trieste/ Udine, Italy*

[37] *University of Tsukuba, Tsukuba, Ibaraki 305, Japan*

[38] *Tufts University, Medford, Massachusetts 02155*

[39] *Waseda University, Tokyo 169, Japan*

[40] *University of Wisconsin, Madison, Wisconsin 53706*

[41] *Yale University, New Haven, Connecticut 06520*

(March 12, 1999)

Abstract

A new technique to measure the ratio of b quark fragmentation fractions in $p\overline{p}$ collisions is described. Using a 70 pb^{-1} sample of low-mass dimuon trigger data recorded with the Collider Detector at Fermilab, we identify B mesons by observing the double semileptonic decays $b \to c\mu X$ with $c \to s\mu X$. By counting the numbers of $K^*(892)^0$, $K^*(892)^+$ and $\phi(1020)$ mesons produced in association with these muon pairs, we measure the ratio of strange to non-strange B meson production to be $f_s/(f_u + f_d) = (21.0 \pm 3.6(\text{stat.})^{+3.8}_{-3.0}(\text{syst.}))\%$. This measurement is the most precise available from hadron collisions to date. Limits on the branching fractions of semileptonic charm meson decays with

$K_1(1270)$, $K_1^*(1410)$ and $K_2^*(1430)$ mesons in the final state are also obtained.

PACS Numbers: 13.60.Le, 14.65.Fy, 13.25.Ft

I. INTRODUCTION

The production of b quarks in hadronic collisions is described by perturbative quantum chromodynamics. The ensuing production of hadrons containing b quarks is described by phenomenological models where a free quark combines with an anti-quark to form a colourless meson [1,2]. In these fragmentation models the flavour of the anti-quark is not predicted a priori and must be taken from experiment. The knowledge of the b quark fragmentation fractions is important for the measurement of other B meson properties such as $B\bar{B}$ oscillations and B hadron lifetimes. A precise determination of f_s will impact numerous other measurements.

The LEP experiments have determined the fragmentation fractions for b quarks produced in the $e^+e^- \to Z^0 \to b\bar{b}$ process. The probabilities f_u and f_d, to produce B^+ or B^0 mesons respectively, are assumed to be equal since the two spectator quarks have nearly equal masses. The combined LEP result is $f_u \equiv f_d = (39.7\ ^{+1.8}_{-2.2})\%$ [3]. The most precise estimate of f_s, the fragmentation fraction into B^0_s mesons, is currently derived from $B\bar{B}$ oscillations using measurements of the flavour averaged mixing parameter $\bar{\chi} = f_s\chi_s + f_d\chi_d$ together with measurements of $\chi_d = x_d^2/[2(1+x_d^2)]$ where $x_d = \Delta m_d \tau_{B^0}$. The result of this determination combined with measurements of f_s from the product branching fraction $f_s \times \mathcal{B}(B^0_s \to D_s^- l^+ \nu X)$ from the LEP experiments [4] gives $f_s = (10.5\ ^{+1.8}_{-1.7})\%$ [3].

A previous measurement of f_s/f_d has also been reported by CDF [5]. Combined with the world average value of f_d, listed above, this measurement results in $f_s = (13.5 \pm 4.3)\%$. It is possible that the fragmentation mechanism at a hadron collider, where the b quarks are produced by gluons in a process with low momentum transfer, is not identical to that observed in high energy e^+e^- collisions, where the b quarks result from a colourless initial state sharing the energy of a Z^0 boson. The relative probability for a b quark to fragment into a B^0_s meson may be different in the two environments. In this paper, we report a measurement of $f_s/(f_u + f_d)$ at a hadron collider.

The measurement described here is based on the observation of double semileptonic B

meson decays produced in $p\bar{p}$ collisions at a center of mass energy of 1.8 TeV. We select decays where first the B meson decays to a muon, neutrino and charm meson. We further require the resulting charm meson decay to a muon that is opposite in charge to the muon resulting from the B meson decay. The decays used in this analysis are:

$$B_s^0 \to \mu^+\nu_\mu \; D_s^- X$$
$$\hookrightarrow \mu^-\overline{\nu}_\mu \; \phi(1020)$$
$$\hookrightarrow K^+K^-;$$

$$B^0, B^+ \to \mu^+\nu_\mu \; D^- X$$
$$\hookrightarrow \mu^-\overline{\nu}_\mu \; K^*(892)^0$$
$$\hookrightarrow K^+\pi^-;$$

$$B^0, B^+ \to \mu^+\nu_\mu \; \overline{D}^0 X$$
$$\hookrightarrow \mu^-\overline{\nu}_\mu \; K^*(892)^+$$
$$\hookrightarrow K_S^0\pi^+$$
$$\hookrightarrow \pi^+\pi^-.$$

In this paper all references to a specific charge state imply the charge conjugate state as well. We use our data to measure the relative fragmentation fractions for strange, B_s^0, and light, B^0 or B^+, meson production by identifying $\phi(1020)$, $K^*(892)^0$ and $K^*(892)^+$ mesons in the final state. In the course of extracting these measurements we also set limits on the relative branching fraction for charm mesons to decay into the heavier strange mesons, $K_1(1270)$, $K_1^*(1410)$ and $K_2^*(1430)$.

This technique of identifying B meson decays with two neutrinos in the final state has recently been used by the CDF collaboration [6]. In general, CDF has identified B mesons using either fully-reconstructed decays containing a charmonium meson (e.g. $B^+ \to J/\psi K^+$ or $B^0 \to J/\psi K_s^0$) or lepton-charm correlations to reconstruct semileptonic B meson decays. In the latter case the charm decays were fully reconstructed such that there was only one missing neutrino in the reconstructed B meson final state. This analysis expands the territory of B physics at CDF by identifying double semileptonic B decays in which neither the parent B meson nor its daughter charm meson are fully reconstructed. CDF can trigger efficiently on dimuon events that constitute the dataset used in this study.

We will describe our experimental approach to measuring $f_s/(f_u + f_d)$ in Section II. In Section III, we describe the experiment, trigger and data collection procedures used for this measurement. In Section IV, we discuss the event selection procedure, the method used to fit the resulting mass distributions and present the observed rates of B mesons. Background calculations are described in Section V. The acceptance calculations are discussed in Section VI. In Section VII we present our results and a detailed breakdown of our sources of uncertainty. We offer our conclusions in Section VIII.

II. THE EXPERIMENTAL APPROACH

The final state strange mesons $K^*(892)^0$, $K^*(892)^+$ and $\phi(1020)$ (denoted from now on as K^{*0}, K^{*+} and ϕ) act as a tag for the initial B mesons species. We determine the rate of B_s^0 production by counting ϕ mesons in double semileptonic dimuon events. We count K^{*0} and K^{*+} candidates to determine the rate of B^0 and B^+ meson production. Throughout this paper, we assume equal fragmentation fractions to both light B mesons, i.e. $f_u = f_d$, and use the symbol $B^{(0,+)}$ to represent an equal mixture of B^0 and B^+ mesons.

We define the total number of b quarks produced in $p\bar{p}$ collisions to be $N(\bar{b}) \equiv 2 \int \mathcal{L}dt \cdot \sigma(p\bar{p} \to \bar{b})$, where $\int \mathcal{L}dt$ is the total integrated luminosity of our sample and $\sigma(p\bar{p} \to \bar{b})$ is the production cross-section for b quarks in our experiment. We also introduce the following notation:

$$\begin{aligned} N(K^{*0}) = N(\bar{b})[&(f_u + f_d) \cdot P(B^{(0,+)} \to K^{*0}) \\ &+ f_s \cdot P(B_s^0 \to K^{*0})], \end{aligned} \tag{1}$$

$$\begin{aligned} N(K^{*+}) = N(\bar{b})[&(f_u + f_d) \cdot P(B^{(0,+)} \to K^{*+}) \\ &+ f_s \cdot P(B_s^0 \to K^{*+})] \end{aligned} \tag{2}$$

$$\begin{aligned} N(\phi) = N(\bar{b})[&f_s \cdot P(B_s^0 \to \phi) \\ &+ (f_u + f_d) \cdot P(B^{(0,+)} \to \phi)]. \end{aligned} \tag{3}$$

The symbols $N(K^{*0})$, $N(K^{*+})$ and $N(\phi)$ represent the event yield of mesons reconstructed in

our data sample. The symbol P represents the product of branching fractions, acceptances and efficiencies for detecting dimuon daughters and reconstructing the final state meson. For instance $P(B^{(0,+)} \to K^{*0})$ can be expressed as:

$$P(B^{(0,+)} \to K^{*0}) \equiv \mathcal{B}(B^{(0,+)} \to D^- \mu^+ \nu X) * \mathcal{B}(D^- \to K^{*0} \mu^- \nu) * \mathcal{B}(K^{*0} \to K^+ \pi^-) * \varepsilon_{trig}(\mu^+, \mu^-) * \varepsilon_{geom}(K^+, \pi^-, \mu^+, \mu^-) * \varepsilon_{track}(K^+, \pi^-, \mu^+, \mu^-), \quad (4)$$

where $\mathcal{B}$ indicates the relevant branching fraction. The symbol ε_{trig} represents the trigger efficiency, ε_{geom} represents the geometric acceptance of the CDF detector for recording and reconstructing the decay products and includes our data selection criteria, and ε_{track} stands for the combined efficiency to reconstruct the four tracks. The other probabilities, P, can be expressed in a similar way. The details of these probability calculations are described in Section VI.

Equations 1-3 are arranged so that the first term in each sum dominates. The second term is a correction for cross-talk that arises from two mechanisms. The $B^{(0,+)}$ mesons can decay to $D_s DX$ final states. When both charm mesons decay semileptonically the resulting $\phi\mu^+\mu^-$ combination can mimic the signature for the decay of a B_s^0 meson. These decays can also result in $K^{*0}\mu^+\mu^-$ and $K^{*+}\mu^+\mu^-$ final states, which constitutes an increase in acceptance. We correct for this by modifying $P(B^{(0,+)} \to K^{*0})$ and $P(B^{(0,+)} \to K^{*+})$ accordingly. There is also cross-talk in the opposite direction, where B_s^0 decays produce $K^{*0}\mu^+\mu^-$ and $K^{*+}\mu^+\mu^-$ combinations via the intermediate decays $D_s^{**-} \to \bar{D}^0 X$ and $D_s^{**-} \to D^- X$. We estimate the cross-talk with a Monte Carlo calculation and correct for it. The corrections described here are discussed in Sec. V B.

The observed rates for K^{*0} and K^{*+} production can be combined into a single measurement of the non-strange B meson yield. We define $N(K^*) \equiv N(K^{*0}) + N(K^{*+})$ and make similar definitions for the related acceptances: $P(B^{(0,+)} \to K^*) \equiv P(B^{(0,+)} \to K^{*0}) + P(B^{(0,+)} \to K^{*+})$ and $P(B_s^0 \to K^*) \equiv P(B_s^0 \to K^{*0}) + P(B_s^0 \to K^{*+})$. Adding Eqns. 1 and 2, we find

$$N(K^*) = N(\bar{b})[(f_u + f_d) \cdot P(B^{(0,+)} \to K^*) +$$

$$+ f_s \cdot P(B_s^0 \to K^*)]. \quad (5)$$

From Eqns. 3 and 5, we derive

$$\frac{f_s}{f_u + f_d} = \frac{N(\phi) \cdot P(B^{(0,+)} \to K^*) - N(K^*) \cdot P(B^{(0,+)} \to \phi)}{N(K^*) \cdot P(B_s \to \phi) - N(\phi) \cdot P(B_s \to K^*)}. \quad (6)$$

The negative terms are corrections for cross-talk between B hadron species while the positive terms are the dominant contribution.

There are several strengths to this experimental approach. By measuring the ratio in Eqn. 6, we avoid systematic uncertainties coming from the uncertainty in the b quark production cross-section. In addition, the detector and trigger inefficiencies that are common to the three signal channels cancel in the ratio. The measurement of the ratio of fragmentation fractions will therefore be more precise than a measurement of f_s alone.

III. DATA COLLECTION

We now turn to a description of the experimental apparatus and the data set used in the extraction of this result.

A. The CDF Detector

The Collider Detector at Fermilab (CDF) is a multi-purpose detector designed to study high energy 1.8 TeV $p\bar{p}$ collisions produced by the Fermilab Tevatron [7]. The coordinate system is defined with the z axis along the proton beam direction, the y axis pointing vertically upwards, and the x axis pointing out of the Tevatron ring. The polar angle θ is defined relative to the z axis, r is the perpendicular radius from this axis, and ϕ is the azimuthal angle. Pseudorapidity is defined as $\eta \equiv -\ln[\tan(\theta/2)]$.

The CDF detector surrounds the beamline with three charged-particle tracking detectors immersed in a 1.4 T solenoidal magnetic field. The tracking system is contained within a calorimeter system that measures the energy of charged and neutral particles over the region

$|\eta| < 4.2$. Charged-particle detectors outside the calorimeter are used to identify muon candidates.

The innermost tracking device is a four-layer silicon microstrip detector (SVX) located in the region between 2.9 and 7.9 cm in radius from the beam axis. The SVX is surrounded by a set of time projection chambers (VTX) that measure charged-particle trajectories to a radius of 22 cm. An 84 layer drift chamber (CTC) measures the particle trajectories in the region between 30 and 132 cm in radius from the beam. This tracking system has high efficiency for detecting charged particles with momentum transverse to the beam $p_T > 0.40$ GeV/c and $|\eta| \lesssim 1.1$. Together, the CTC and SVX measure charged particle transverse momenta with a precision of $\sigma_{p_T} \sim \sqrt{0.0066^2 + (0.0009 p_T)^2}$ (with p_T in units of GeV/c). The impact parameter resolution is $\sigma_d = (13 + 40/p_T)\mu$m for SVX and CTC combined.

The central muon detection system consists of four layers of planar drift chambers separated from the interaction point by approximately five interaction lengths of material. To reduce the probability of misidentifying penetrating hadrons as muon candidates in the central pseudorapidity region $|\eta| < 0.6$, an additional four layers of chambers are located outside the magnet return yoke (corresponding to about three interaction lengths of material at $\theta = 90°$). A further set of chambers is located in the pseudorapidity interval $0.6 < |\eta| < 1.0$ to extend the acceptance of the muon system. These systems are capable of detecting muons with $p_T \gtrsim 1.4$ GeV/c in a pseudorapidity interval of $|\eta| < 1.0$.

B. The Trigger

A common feature of the three B meson decay modes studied here is the presence of a $\mu^+\mu^-$ candidate consistent with a double semileptonic B meson decay. Dimuon candidates were selected using a three-level trigger system. The first level trigger required that two candidates be observed in the muon chambers. For each muon candidate the first level trigger efficiency rose from ~40% at $p_T = 1.5$ GeV/c to ~93% for muons with $p_T > 3.0$ GeV/c. The second level trigger required two or more charged particle tracks observed in the CTC using

the central fast track processor (CFT) that performed a partial reconstruction of all charged tracks above a transverse momentum of $\sim$2 GeV/c. The CFT tracks were required to match within 15° in azimuth of the muon candidates found by the first level trigger. The third level trigger confirmed with greater precision that two reconstructed CTC tracks matched with two tracks in the muon chambers, that the dimuon invariant mass was between 1.0 and 2.8 GeV/c^2, and that the p_T of both muon candidates was greater than 2.1 GeV/c .

IV. DATA SELECTION

The data used in this study correspond to an integrated luminosity of 70 pb^{-1} and were collected between November 1994 and July 1995. Following the online data collection, additional requirements were made offline to identify the signals and to reduce the backgrounds.

A. Charged Particle and Primary Vertex Reconstruction

Candidate muon, kaon and pion trajectories were reconstructed in the CTC and VTX and extrapolated into the SVX to find additional hit information associated with the track. We required each CTC track candidate to be of high quality by requiring the track to have a minimum number of hits in the CTC. We also required that at least two SVX hits be associated with the CTC track. If one of these hits was shared with another track, a third hit was required. We do not perform explicit hadron identification, but assign kaon and pion mass hypotheses as appropriate for our final state signatures. We also required that kaon and pion candidates have a measured transverse momentum $p_T > 0.5$ GeV/c in order to be reconstructed with high efficiency. For pions from the decay $K^0_S \to \pi^+\pi^-$ needed for the reconstruction of the K^{*+} signal, the single track p_T threshold was lowered to 0.4 GeV/c. All charged particle tracks used to reconstruct the strange hadron decay daughters were required to have SVX information associated with them except for $K^0_S \to \pi^+\pi^-$ candidates where only CTC information was used to allow for the long flight distances of the K^0_S.

In order to identify B meson decays by their displaced vertices, we first need to reconstruct the primary interaction vertex. We used the charged particle tracks reconstructed in the VTX detector to determine the location of $p\bar{p}$ interactions. In our data sample an average of 2.5 $p\bar{p}$ interactions occurred in each crossing. If there are several primary vertex candidates, we choose the one closest to the muon candidates' intercepts with the beam line. These tracks, when projected back to the known beam axis, determine the longitudinal locations of candidate primary interactions. The transverse position of the primary vertex was most accurately determined by using the average beam trajectory through the detector and the longitudinal primary vertex position. The beam line was stable over the period that a given $p\bar{p}$ beam was stored in the Tevatron. The uncertainty in the transverse position of the primary vertex was dominated by the transverse profile of the beam that had a Gaussian distribution with a width of 25 μm in both the x and y directions [8].

B. Dimuon selection

To identify muon candidates and reduce their rate from sources such as K meson decay-in-flight, we required that each candidate observed in the muon chambers be associated with a matching CTC track candidate. These matches were required to pass a maximum χ^2 cut of 9 and 12 in each of the ϕ and z views, respectively. Muon candidates were required to have deposited a minimum energy of 0.5 GeV in the hadronic compartment of the calorimeter. Each muon track must also have been observed in the SVX detector. Finally, we confirmed the trigger criteria by requiring p_T greater than 2.1 GeV/c for each muon candidate and a dimuon mass between 1.0 GeV/c^2 and 2.8 GeV/c^2.

C. Reconstruction of Double Semileptonic Decays

We search for B meson decays resulting in a muon, a neutrino and a charm meson such as the D^-, $\bar{D}^0$ or D_s^-. These charm mesons, in turn, decay semileptonically to produce a second muon, a vector meson (ϕ, K^{*0} or K^{*+}) and a neutrino. We label the muon from

a B meson decay μ_B and the muon from a charm decay μ_D and denote the vector meson as "K". We use a Monte Carlo calculation, described in Section VI B, to determine that 98% of the time $M(\text{"}K\text{"}\mu_D) < M(\text{"}K\text{"}\mu_B)$ where M represents the invariant mass of the system. To reduce the number of combinations in our signal reconstruction, we choose one of the muons, the one with lower $M(\text{"}K\text{"}\mu)$, as the candidate for μ_D. Distinguishing μ_B from μ_D also enables us to improve our decay vertex fit hypothesis as described below. The charge of the muon from the charm decay is essential for the reconstruction of K^* meson signals. Having made this choice we require $M(\text{"}K\text{"}\mu_D) < 1.7$ GeV/c^2, consistent with the $D \to \text{"}K\text{"}\mu\nu$ decay of our signal. In order to reduce combinatorial background we also require $p_T(\text{"}K\text{"})$ greater than 2 GeV/c.

To further reduce background, we confirm the $B \to D \to$ "K" meson double semileptonic decay hypothesis by making additional requirements on the vertex topology of the candidate events. The vertex topology of the signal is shown schematically in Fig. 1. In our reconstruction the "K" meson and μ_D candidates are constrained to come from a common vertex — the point of D meson decay. The D meson flight direction is not known exactly because of the missing neutrino, but the vector sum of the momenta of μ_D and "K" gives a good approximation. The B meson decay vertex is determined by the intersection of the μ_B track and the μ_D "K" trajectory extrapolated from the D meson decay vertex, with the μ_B track. We place further requirements on the decay vertices to enhance the selection of long-lived B meson decays. The apparent B meson flight distance, $L_{xy}(B)$, is the distance from the interaction region to the reconstructed decay point in the plane transverse to the beam direction, projected onto the transverse momentum of the B meson candidate. We require $L_{xy}(B)$ to be greater than three times its uncertainty. The most probable L_{xy} uncertainty is ~ 70 μm. The flight distance of the D meson, $L_{xy}(D)$, is also required to be further from the primary vertex than the B meson decay point ($L_{xy}(D) > L_{xy}(B)$) as would be expected for a sequential double semileptonic decay.

We impose one additional requirement to reduce combinatorial backgrounds. For real B meson decays, we expect the B meson to carry most of the energy of the b quark. We

therefore define an isolation variable

$$I_B \equiv \frac{|\vec{P}_B|}{|\vec{P}_B| + \sum_i \vec{P}_i \cdot \vec{u}}, \tag{7}$$

where $\vec{P}_B$ is the momentum sum of the reconstructed B meson decay daughters. The sum in the denominator is over charged particles not used to reconstruct the B candidate, with momentum vectors $\vec{P}_i$, contained within a cone in $\eta - \phi$ space of radius $R \equiv \sqrt{(\Delta\phi)^2 + (\Delta\eta)^2} = 1.0$ about an axis defined by the direction of the B meson candidate momentum. The unit vector, $\vec{u}$, points along $\vec{P}_B$, i.e. $\vec{u} \equiv \vec{P}_B/|\vec{P}_B|$. In order to avoid including charged particles that resulted from interactions in the $p\bar{p}$ collision not associated with the B meson candidate, the sum is performed only over those charged tracks that passed within 5 cm along the z axis of the primary vertex location. Since B meson decays have large values of I_B, we have imposed the requirement $I_B > 0.50$ to suppress background events.

We allow multiple double semileptonic decay candidates in single events. Choosing only one candidate per event would introduce an inefficiency that could bias the yield determination as it depends on the size of the un-modeled combinatorial background. We correct for the resulting increase in combinatorial background in the way we create the fitted lineshapes using data distributions (see below).

D. The ϕ, K^{*0} and K^{*+} Event Yields

The event samples described above are further subdivided into the event classes outlined in Section I by identifying ϕ mesons, K^{*0} mesons and K^{*+} mesons associated with dimuons in the final state. We fit the invariant mass distributions of the strange meson daughters to extract our candidate yields. In this section we present fits to distributions associated with opposite-sign (OS) dimuons, where we expect to see the signals from B meson decay. The distributions associated with like-sign dimuons were also studied in order to search for potential backgrounds. The results of these background studies are presented in Section V E.

The distributions are fit with a sum of a signal distribution and a polynomial representing the combinatorial background. The signal distribution is described by a template obtained from Monte Carlo calculations, leaving the amplitude as the only free parameter describing the signal in our fit. The Monte Carlo shape prediction includes the width of the strange meson resonance, the kinematics of the double semileptonic decay and detector effects, as described in Section VI B. The fit maximises an unbinned likelihood that compares our observed data to the predicted mass distributions.

Figure 2 shows the ϕ meson signal, observed in the K^+K^- mass distribution. The crosses represent the data distribution while the solid line shows the fit described by a Breit-Wigner lineshape smeared by our reconstruction resolution. The dashed line shows the extrapolation of the polynomial background under the signal peak. From this sample we measure a yield of $N(\phi) = 103 \pm 16$ events.

A K^{*0} signal is visible in the $K^+\pi^-$ invariant mass distribution shown in Fig. 3. The charge of the charm muon (μ_D) designates the track with a charge opposite that of μ_D to be the kaon and the remaining track is then a pion. Those combinations form the right-sign distribution (RS). Swapping the K π particle assignments results in a wrong-sign (WS) distribution. A simultaneous fit of both distributions gives us additional constraints on the combinatorial background.

In Fig. 3 the crosses show the data distribution and the solid line shows the combined fit. The RS distribution has three components: a Breit-Wigner K^{*0} signal (dashed line), a "satellite" structure peaking near threshold (dotted line) and a combinatorial background (dashed-dotted line). The "satellite" is produced by combinations of charged kaons, primarily from $\bar{D}^0 \to K^+\mu^-\bar{\nu}$ decays, with pions of low transverse momentum, mostly from $D^{*-} \to \bar{D}^0\pi^-$ decays. The wrong-sign distribution has three components: a reflection of the K^{*0} signal produced by mistaken $K-\pi$ mass assignments (dashed line), a reflection of the "satellite" peak (dotted line) and a combinatorial background (dashed-dotted line). The combinatorial background does not contain kaons correlated in charge with μ_D. Thus, by construction, it has the same shape in the RS and WS distributions. We perform a simul-

taneous fit to the RS and WS distributions with the combinatorial background constrained to be the same in both distributions. The templates for the mass shape of the signal, the "satellite" and their reflections were produced by a Monte Carlo calculation. The fit returns a yield of $N(K^{*0}) = 683 \pm 55$ events.

To measure the K^{*+} signal we reconstruct $K^0_S \to \pi^+\pi^-$ decays. We fit the K^0_S decay vertex using opposite-charge track pairs. We require the K^0_S transverse decay length to be greater than 2 cm and less than 100 cm. We also require $|M(\pi^+\pi^-) - M(K^0_S)| < 20$ MeV. The reconstructed trajectory of the K^0_s meson is used with the trajectories of the μ_D and $\pi^\pm$ candidates, to fit the charm decay vertex ($\bar{D}^0 \to K^{*+}\mu^-\bar{\nu}, K^{*+} \to K^0_S\pi^+$) (see Fig. 1). The subsequent fit of the B meson decay vertex is the same as in the other two signal channels.

The $K^0_S\pi^+$ mass distributions are shown in Fig. 4 together with the results of the fits to the RS and WS distributions. The right sign combinations are those for which the charge of the reconstructed K^{*+} is opposite to that of μ_D. Unlike the K^{*0} fit, there is no ambiguity in the $K - \pi$ mass assignment, hence no reflection of the signal into the WS distribution exists. However the background can have components correlated in charge to μ_D. In the simultaneous fit of the RS and WS distributions, we use the same background shape but allow the relative normalisation to vary. The fit returns a yield of $N(K^{*+}) = 94 \pm 21$ events.

It should be noted that we do not expect a significant "satellite" peak in the $M(K^0_S\pi^+)$ distribution because of differences in the decays of $\bar{D}^{*0}$ and D^{*-} mesons. The D^{*-} mesons decay to $\bar{D}^0\pi^-$ about two thirds of the time. As a consequence, $\bar{D}^0$ mesons from semileptonic B meson decays are often produced in coincidence with soft charged pions. The $\bar{D}^{*0}$ mesons, on the other hand, cannot decay to $D^-\pi^+$. Therefore D^- mesons from semileptonic B meson decays are only rarely produced in coincidence with soft charged pions (via D^{**} decays). This asymmetry explains why we find a large satellite structure associated with the K^{*0} signal but we do not observe an equivalent structure with the K^{*+} signal.

V. BACKGROUNDS

The final state B meson decays studied here involve two missing neutrinos. Therefore many of the usual constraints on potential backgrounds are weaker than in cases where the final state is more fully reconstructed. We quantify potential sources of background in Sections V A to V D. We also describe fits to the data distributions associated with like-sign dimuons as an additional check against unexpected backgrounds in Section V E.

A. Heavy Kaons

In the semileptonic decay of charm mesons there is a difference between the sum of measured branching fractions to particular channels and the measured total semileptonic branching fraction [3]. This deficit is large enough to accommodate a significant branching fraction for the decays $D \to K_x \mu\nu$, where K_x could represent $K_1(1270)$, $K_1^*(1410)$ or $K_2^*(1430)$. The semileptonic charm decay to K_x could be followed by a strong decay $K_x \to K^* X$, where K^* represents K^{*0} or K^{*+}, contributing to the signals we are studying and providing a potential background to the measurement. In doing this we assume the spectator model holds in these decays constraining $\Gamma(D^- \to K_x^0 \mu^- \bar{\nu}) = \Gamma(\bar{D}^0 \to K_x^+ \mu^- \bar{\nu})$.

We have used our data sample to set limits on the production of the heavy strange mesons, K_x, in charm meson decays and, in turn, have used these to estimate systematic uncertainties on our measurement of $f_s/(f_u + f_d)$. We fully reconstruct other candidate decay modes of these heavier strange mesons to obtain limits on ratios such as

$$\beta \equiv \frac{\mathcal{B}(D \to K_x \mu\nu)}{\mathcal{B}(D \to K^{*0} \mu\nu)}. \tag{8}$$

The decay $D \to K_2^*(1430)\mu X \to K^+\pi^-\mu X$ should manifest itself as a resonance in the high end tail of the $K^+\pi^-$ mass distribution. We use the same selection criteria as for our K^{*0} signal reconstruction with one exception. The cut $M(K\pi\mu_D) < 1.7$ GeV/$c^2$is removed in order to enhance acceptance for potential $K_2^*(1430)$ signal at high $M(K\pi)$ masses. The high mass region of the $K\pi$ mass distribution is shown in Fig. 5. The dashed line in Fig. 5

shows the contribution expected from the $K_2^*(1430)$ decay if it were present at a rate thirty times the limit we are able to set (see below). We fit the observed $M(K\pi)$ distribution using a Breit-Wigner signal distribution and a polynomial background term. The fit returns 0 ± 20 events. We conclude there is no evidence of the decay $D \to K_2^*(1430)\ \mu\nu_\mu$.

We calculate a limit on the ratio of branching fractions from the fit result. Our 95% confidence level (C.L.) limit is the value of β for which the probability of obtaining a $K_2^*(1430)$ signal not larger than that we observe is 5%. This probability is calculated using a Monte Carlo method that includes the uncertainties on the branching fractions and the statistical uncertainty on the fit, assuming that both of them are distributed as Gaussians. We obtain the limit of

$$\frac{\mathcal{B}(D \to K_2^*(1430)\mu\nu)}{\mathcal{B}(D \to K^{*0}\mu\nu)} < 0.19 \text{ (95\% C.L.)}. \tag{9}$$

The $K_1(1270)$ and $K_1^*(1410)$ mesons do not have large branching fractions to $K\pi$, so we search for them using the decay modes $K_x^0 \to K^{*+}\pi^- \to K_s^0\pi^+\pi^-$ and $K_x^+ \to K^{*0}\pi^+ \to K^+\pi^-\pi^+$. The $M(K_S^0\pi^+\pi^-)$ distribution has inherently less combinatorial background due to the constraint provided by the reconstructed $K_S^0 \to \pi^+\pi^-$ decay. The $M(K^+\pi^-\pi^+)$ distribution has more background because every track is a potential charged kaon candidate. We therefore obtain more stringent limits using the $M(K_S^0\pi^+\pi^-)$ distribution and we concentrate on it in the following.

The search is similar to our reconstruction of the $K^{*+} \to K_S^0\pi^+$ signal with one additional charged particle originating from the charm decay vertex. The $K_S^0\pi\pi$ mass distribution observed in our data is shown in Fig. 6. The open histogram shows the RS combinations $(K^+\pi^-)$ and the hatched histogram shows the WS $(K^{*+}\pi^+)$ combinations. The dashed line shows the contribution to the RS combinations expected from the $K_1^*(1410)\mu\nu_\mu$ decay if it had a branching fraction equal to the 95% C.L. limit we are able to set below.

We find two RS and four WS combinations with masses between 1.18 and 1.66 GeV/c^2. We take the number of WS combinations as a measurement of our combinatorial background. We determine the limit using the method described in [9], applicable to Poisson processes

with background. We define the 95% C.L. limit to be the ratio of branching fractions where

$$\frac{\mathcal{P}(N_{BACK} + N_{SIG} \leq N_{OBS})}{\mathcal{P}(N_{BACK} \leq N_{OBS})} = 5\%. \tag{10}$$

The symbol $\mathcal{P}(N_{BACK}+N_{SIG} \leq N_{OBS})$ represents the probability of observing no more than two candidates when both the heavy strange meson signal and the combinatorial background are present, while $\mathcal{P}(N_{BACK} \leq N_{OBS})$ represents the same number of RS candidates from background only. This procedure is more conservative than a straightforward determination of $\mathcal{P}(N_{BACK} + N_{SIG} \leq N_{OBS}) = 5\%$. We calculate the probabilities, $\mathcal{P}$, using a Monte Carlo method, including the uncertainties on branching fractions and Poisson fluctuations. Our generalisation of the method described in [9] consists of using Monte Carlo to sum the Poisson series taking into account the systematic uncertainties.

Table II summarizes the limits on the ratio of branching fractions obtained from the data. An upper limit on the contribution from these heavier kaon decays to our K^{*+} and K^{*0} signals can be computed from the limits on the branching fractions. Our limits are significantly more stringent than those that could be derived from the difference between the inclusive branching fractions and the sum of the exclusive branching fractions that have been observed. As such they provide new information on the modes $D \to K_x \mu\nu$.

We compute an 84.1% C.L. upper limit in the ratios of branching fractions for the corresponding 1σ systematic uncertainty in our measurement of $f_s/(f_u + f_d)$. The resulting uncertainty on $f_s/(f_u+f_d)$ is one sided because the potential effect of heavy kaon decays can only increase our observed yields of $K^{*0}\mu^+\mu^-$ and $K^{*+}\mu^+\mu^-$. The fractional uncertainty on $f_s/(f_u + f_d)$ is listed in Table II. The limits on K_x production are not independent. The least stringent limit is obtained by assuming the contribution from heavier strange mesons all comes from $K_1^*(1410)$ decays. We therefore use the limit on possible $K_1^*(1410)$ production as our final contribution to the systematic uncertainty on the measurement of $f_s/(f_u + f_d)$.

B. b-Hadron Decays with Dimuons

Several other backgrounds resulting from $b\bar{b}$ production were determined from Monte Carlo calculations to determine their relative abundance in our final event yields.

Decays such as $B^{(0,+)} \to D_s DX$ are a potential source of dimuon candidates accompanied by ϕ and K^* mesons. Cross-talk between the channels can result from non-strange B meson decays producing a ϕ $\mu^+\mu^-$ signal satisfying the selection criteria. The $K^*\mu^+\mu^-$ combinations from $B^{(0,+)} \to D_s DX$ decays constitute an increase in acceptance for light B mesons. We correct for both these effects using a Monte Carlo simulation to estimate that 4% of the ϕ meson signal and less than 1% of the K^* meson signals result from such intermediate states.

There can also be cross-talk from B_s^0 meson decays mimicking non-strange B meson signals through decays such as $D_s^{**} \to DX$. These additional contributions introduce a 2.1% contribution to our K^{*0} signal and a 2.6% contribution to our K^{*+} signal. We correct for them by introducing the terms $P(B_s^0 \to K^{*0})$, $P(B_s^0 \to K^{*+})$ and $P(B^{(0,+)} \to \phi)$ in Eqns. 1, 2 and 3, respectively. The actual contributions from these processes depend on the value of $f_s/(f_u + f_d)$. The values quoted above are for our measured value of $f_s/(f_u + f_d)$.

Finally, we have considered backgrounds from decays such as $\Lambda_b^0 \to pD^0\mu^-\bar{\nu}$ where the charm meson can decay semileptonically to yield a strange meson. These decays have not been observed, but a limit exists on a more inclusive partial width $\Gamma(\Lambda_b^0 \to pD^0\mu^-\bar{\nu}X)$ [10]. Assuming that $\mathcal{B}(\Lambda_b^0 \to pD^0\mu^-\bar{\nu})$ saturates the published limit, we obtain an upper limit of a 2.0% contribution to our K^{*+} signal from such Λ_b^0 baryon decays. We do not correct for this effect but include the influence of this potential background in our systematic uncertainties.

C. Other $b\bar{b}$ Backgrounds

We have also studied $b\bar{b}$ backgrounds that can arise from the mis-reconstruction of our final states. There is the possibility that one or both of the muon candidates can be a misiden-

tified hadron. Fake muons come from the decay-in-flight of kaons and pions as well as from hadrons that pass through the calorimeter without interacting ("punch-through"). The probabilities of these processes were predicted by a Monte Carlo model and verified with our data [11]. We find that a charged pion has an 0.8% probability of being misidentified as a muon due to a decay-in-flight. The corresponding misidentification probability for a kaon decay-in-flight is 1.5%. These probabilities are essentially independent of momentum in our range of interest. The punch-through probabilities are 0.15% for $\pi^{\pm}$ or K^{-} mesons, and 1.6% for K^{+} mesons. These misidentification probabilities are sufficiently low that double fake muons, where the two fake muons occur independently, are negligible. However events where one muon is real and the other is fake form a non-negligible background.

The dominant contribution to the other $b\bar{b}$ backgrounds comes from semileptonic B meson decays producing one real muon and we misidentify the pion from the D meson decay as the second muon. Such combinations arise from the decay $B \to D\mu X$ with $D \to$ "K"$\pi\pi$, where one of the pions can be neutral. Background from $D \to$ "K"π decays, where the pion is misidentified as a muon, is efficiently removed by the requirement $M(\text{"}K\text{"}\mu_D) < 1.7$ GeV/c^2.

Combinations from $D \to$ "K"$\pi\pi^0$, with the charged pion being misidentified as a second muon, result in opposite-sign dimuon candidates. Not only is the charge correlation the same as our signal, but the vertex topology is identical as well. Our muon identification provides the only suppression of these backgrounds. We rely on a Monte Carlo calculation to determine the fake muon backgrounds. This background forms $\sim 85\%$ of the other $b\bar{b}$ background in all three channels.

The remaining $\sim 15\%$ consists mostly of cases where the charged daughters of the B meson candidate are products of two b hadron decays. In those events one b quark produces the "K" while one or both of the muons result from the semileptonic decay of the other $\bar{b}$ quark. We have also studied the backgrounds that arise when one of the muons or the "K" is produced promptly as a result of the heavy quark fragmentation process. We find this is a negligible contribution to the background. The poorly known branching fractions of decays such as $D \to$ "K"$\pi\pi$ result in the large uncertainties on these estimates and contribute to

the systematic uncertainty on $f_s/(f_u + f_d)$.

D. $c\bar{c}$ Background

We estimate the background from $c\bar{c}$ pairs produced by gluon splitting. In these cases the c and $\bar{c}$ quarks are not produced back-to-back but side-by-side in a single jet. Thus if both charm hadrons decay to a muon, a low mass dimuon candidate could be formed producing "K"$\mu^+\mu^-$ combinations passing the selection criteria. However, charm decays result in lower daughter momenta and shorter flight distances than $b\bar{b}$ events. We find the ratio $N(K^{*0}\mu^+\mu^-)_{c\bar{c}}/N(K^{*0}\mu^+\mu^-)_{b\bar{b}} = (0.3 \pm 1.2)\%$ where the precision is limited by the Monte Carlo statistics in the calculation. We conclude that the $c\bar{c}$ background is negligible.

E. Cross Check of Remaining Backgrounds from Data

We examine the $M(K^+K^-)$, $M(K^+\pi^-)$ and $M(K^0_S\pi^+)$ distributions associated with like-sign dimuons for evidence of "K" production. A "K" signal reconstructed in any of these distributions would be evidence for an unpredicted background. The three mass distributions and corresponding fits are shown in Fig. 7. We find that the ϕ, K^{*0} and K^{*+} signals seen in association with like sign dimuon candidates are consistent with zero. The yields with opposite sign muon pairs (signal), like sign muon pairs (this cross-check) and other backgrounds described above are listed for each of the three signal channels in Table I.

VI. ACCEPTANCE AND EFFICIENCY CORRECTIONS

The observed event yields for the three final states, corrected for the backgrounds described above, need to be further corrected for the acceptance of the detector, the efficiencies of the various reconstruction stages and selection requirements, and for the trigger efficiency. To study the kinematic and geometric acceptances we used a Monte Carlo calculation of b quark production and B meson decay followed by a simulation of the detector response.

We used both Monte Carlo calculations and measurements from our data to estimate the remaining efficiencies.

A significant advantage of measuring a ratio of fragmentation fractions using similar decays is that many of the acceptances and efficiencies cancel. For example the overall b quark production cross-section leading to light $B^{(0,+)}$ meson and B_s^0 meson final states will be the same. Different signal decays also have very similar triggering probabilities. We have studied the effect of the different phase-space available for double semileptonic muon decays due to the different B meson masses and find this to be a negligible correction to our result. Furthermore, the track finding efficiencies for the "K" decay products almost cancel in the ratio. In two of the three cases, we reconstruct the final "K" from two charged particles ($\phi \to K^+K^-$ and $K^{*0} \to K^+\pi^-$). In the third channel we reconstruct three final state charged particles ($K^{*+} \to K_S^0\pi^+; K_S^0 \to \pi^+\pi^-$). In order to properly include the effect of this difference on our result we have studied the relative reconstruction efficiency for single charged tracks compared to $K_S^0 \to \pi^+\pi^-$ decays, as described in Section VI C.

A. Monte Carlo Simulations

The Monte Carlo calculation used a model for b quark production based on a next-to-leading-order QCD calculation [12]. This calculation employed the MRSD0 parton distribution functions [13] to model the kinematics of the initial state partons, a b quark mass of $m_b = 4.75$ GeV/c^2 and a renormalisation scale of $\mu = \mu_0 \equiv \sqrt{m_b^2 + k_T^2}$, where k_T is the momentum of the b quark transverse to the plane of the initial-state partons. We generated b quarks with $p_T > 8.0$ GeV/c. This kinematic limit on the Monte Carlo calculation was sufficiently loose so that there were no biases in the B meson kinematic distributions after the application of the selection criteria used in this analysis. The average p_T of the B mesons reconstructed in this analysis is about 20 GeV/c. The b quarks were fragmented into B mesons according to a model that used the Peterson fragmentation function [14] with the Peterson ϵ_b parameter set to 0.006 [2]. The B mesons were decayed using a model devel-

oped by the CLEO collaboration [17] with all the branching ratios and angular distributions updated to the most recent results of the Particle Data Group [3].

For background calculations reported in section V D we need to simulate the production of $\bar{c}c$ quark pairs. We use the ISAJET Monte Carlo program [15], because it models the production of $\bar{c}c$ in the same hemisphere via the process of gluon splitting, which is a potential source of background to our B-meson decay signal. We also use the PYTHIA Monte Carlo program [16], to model charged particles produced promptly in the fragmentation of heavy quarks. Both of these backgrounds were negligible.

Events generated with the above Monte Carlo simulations and according to branching fraction prescriptions described below were passed through a simulation of the CDF detector that included the geometry of all the sub-detector elements, the interaction of the charged particles with the material in the detector, the resolution of the different tracking elements and the efficiency of the trigger. The resulting simulated event yields were used, together with the branching fractions listed below, to calculate the acceptance and cross-talk terms in Eqns. 1 to 3. The same Monte Carlo tools were used to calculate backgrounds described in Section V. The uncertainties associated with the various input parameters create uncertainties in the resulting acceptances and are included in Table VI.

B. Acceptance Calculations

We assume equal production rates of B^0 and B^+ mesons; $f_d = f_u$. We use the spectator model to calculate the branching fractions of semileptonic decays. This implies the following relationships:

$$\Gamma(B^0 \to D^- \mu^+ \nu) = \Gamma(B^+ \to \bar{D}^0 \mu^+ \nu) = \Gamma(B_s^0 \to D_s^- \mu^+ \nu), \tag{11}$$

$$\Gamma(B^0 \to D^{*-} \mu^+ \nu) = \Gamma(B^+ \to \bar{D}^{*0} \mu^+ \nu) = \Gamma(B_s^0 \to D_s^{*-} \mu^+ \nu), \tag{12}$$

$$\Gamma(B^0 \to D^{**-} \mu^+ \nu) = \Gamma(B^+ \to \bar{D}^{**0} \mu^+ \nu) = \Gamma(B_s^0 \to D_s^{**-} \mu^+ \nu), \tag{13}$$

$$\Gamma(D_s^- \to \phi \mu^- \bar{\nu}) = \Gamma(D^- \to K^{*0} \mu^- \bar{\nu}) = \Gamma(\bar{D}^0 \to K^{*+} \mu^- \bar{\nu}), \tag{14}$$

where Γ is the partial width of the specific decay mode. Since we measure a ratio of yields, we need only know ratios of the branching fractions. In the spectator model these ratios of branching fractions are given by ratios of the partial widths (eqns. 11 to 14) that can in turn be related to the ratios of the B and D meson lifetimes. The measured branching fractions are consistent with this model, but known less precisely than B and D meson lifetimes. We use the world average bottom and charm lifetimes listed in Table III and the world average branching fractions listed in Table IV [3].

The contributions from different intermediate charm states were combined in order to calculate the probabilities, P, in Eqns. 1, 2 and 3. We introduce the following symbols:

$$\begin{aligned} f &\equiv \frac{\mathcal{B}(B \to D\mu\nu)}{\mathcal{B}(B \to \mu\nu X)}, \\ f^* &\equiv \frac{\mathcal{B}(B \to D^*\mu\nu)}{\mathcal{B}(B \to \mu\nu X)}, \\ f^{**} &\equiv \frac{\mathcal{B}(B \to D^{**}\mu\nu)}{\mathcal{B}(B \to \mu\nu X)}. \end{aligned} \tag{15}$$

The fraction f^{**} also includes all non-resonant contributions. By definition $f + f^* + f^{**} \equiv 1$. We have calculated the contributions to the total acceptance that come from the different charm states (D, D^*, D^{**}). We vary f, f^* and f^{**} to derive systematic uncertainties introduced by the accuracy with which they are known. The ratios necessary for the extraction of $f_s/(f_u + f_d)$ can be derived from the world-averages taken from [3] and listed in Table V. Combining the first two lines of Table V using a weighted average we obtain $f = 0.187 \pm 0.022$. The last two lines of Table V give $f^* = 0.452 \pm 0.038$. We determine f^{**} using the constraint $f + f^* + f^{**} \equiv 1$. The change in acceptance resulting from the uncertainties on f, f^* and f^{**} is included in our systematic uncertainty on $f_s/(f_u + f_d)$.

C. Reconstruction Efficiencies

While the two main "K" decay modes ($\phi \to K^+K^-$ and $K^{*0} \to K^+\pi^-$) used in this analysis involve only the reconstruction of two charged particle tracks, the third requires the reconstruction of a long-lived $K^0_S \to \pi^+\pi^-$ decay instead of a single charged particle.

This topological difference introduces an additional tracking efficiency factor that does not cancel in the ratio of acceptances. Because we are measuring a ratio of branching fractions we need only compute the ratio of acceptances. The correction factor of interest is $\varepsilon(K^0_S \to \pi^+\pi^-)/\varepsilon(1\,\text{track})$, where the numerator represents an average probability of reconstructing the two tracks and the decay vertex in the K^0_S topology. The denominator is the track finding efficiency for single tracks, selected with the same criteria as our K^{*0} and ϕ signals.

We have studied the K^0_S finding and reconstruction efficiency [5] by merging simulated $K^0_S \to \pi^+\pi^-$ decays with our tracking data. We find an efficiency of 86% for finding both daughters of the long-lived K^0_S mesons. This study was done for the initial, low-luminosity, data-taking period for which the overall tracking efficiency was best understood. We rely on data to study the variation of the K^0_S finding efficiency in the data taken later at higher luminosities. We do this by measuring the inclusive K^0_S yield per interaction as a function of time. Given that the production rate of K^0_S mesons is constant, we can measure any additional inefficiency at higher luminosity. This additional correction factor, averaged over the data taking time of the double semileptonic decay sample, was 0.77. The combined relative reconstruction efficiency for K^0_S mesons was $\varepsilon(K^0_S \to \pi^+\pi^-) = 0.86 \times 0.77 = 0.66$.

For the single track efficiency we use the result of an embedding study for promptly produced tracks, covering the entire data taking period including the variations in luminosity [18]. There we obtained $\varepsilon(1\,\text{track}) = 0.93$. Thus the relative tracking efficiency correction was $\varepsilon(K^0_S \to \pi^+\pi^-)/\varepsilon(1\text{track}) = 0.71 \pm 0.30$. The uncertainty on this efficiency includes contributions from all of the above inputs but is dominated by our lack of understanding of the K^0_S finding efficiency as a function of instantaneous luminosity. Because of the small number of observed K^{*+} candidates compared to K^{*0}, the systematic uncertainty on $f_s/(f_u + f_d)$ from the K^0_S finding efficiency is small. It is included in Table VI.

VII. RESULTS

Using Eqn. 6 we can compute the final result from the measured event yields and calculated acceptances. We measure

$$f_s/(f_u + f_d) = (21.0 \pm 3.6(\text{stat.}) \, ^{+3.8}_{-3.0}(\text{syst.}))\%, \tag{16}$$

where the first uncertainty is statistical and the second is systematic. Table VI lists all sources of uncertainty and their contributions to the final result expressed as a fraction of the measured $f_s/(f_u + f_d)$ value. We combine these in quadrature to determine the total uncertainty.

Our largest uncertainty is the statistical precision on the ϕ meson signal. The largest systematic uncertainties result from our background estimates. Our limits on the heavier strange meson backgrounds result in an asymmetric systematic uncertainty. Uncertainties on the background corrections to the ϕ, K^{*+} and K^{*0} signals are partially correlated because they all rely on the same muon misidentification probability. The combined systematic uncertainty associated with the "total background" takes this correlation into account.

The next largest systematic uncertainty is related to the composition of semileptonic B meson decays. The uncertainties on f, f^* and f^{**} affect the precision with which we can calculate the acceptance. Uncertainties on the B and D meson lifetimes also affect the acceptance because we use branching fractions derived from the spectator model. The reconstruction efficiency for K^0_s mesons also introduces an uncertainty, as described in Section VI C. The remaining systematic uncertainties come from the branching fractions of $K^0_S \to \pi^+\pi^-$ and $\phi \to K^+K^-$ decays, although these are relatively small.

VIII. CONCLUSION

We have reported a measurement of b quark fragmentation fractions using a sample of 70 pb^{-1} of low mass dimuon data. Using a new technique B mesons are identified through double semileptonic decays $b \to c\mu X$ followed by $c \to s\mu X$. Reconstructing $K^*(892)^0$,

$K^*(892)^+$ and $\phi(1020)$ mesons produced in association with these muon pairs we obtain high statistics samples of B^0, B^+ and B_s^0 mesons. From the yield of $K^*(892)^0$, $K^*(892)^+$ and $\phi(1020)$ candidates we extract a measurement of the ratio of fragmentation fractions for b quarks of $f_s/(f_u + f_d) = (21.0 \pm 3.6(\text{stat.})^{+3.8}_{-3.0}(\text{syst.}))\%$. This is the most precise measurement of this fragmentation fraction at hadron colliders to date. In addition, limits on the branching fractions of semileptonic charm meson decays with $K_1(1270)$, $K_1^*(1410)$ and $K_2^*(1430)$ mesons in the final state have been obtained.

The measurements of f_u, f_d and f_s extracted from high energy e^+e^- collisions [3] give $f_s/(f_u + f_d) = (13.2\ ^{+2.4}_{-2.2})\%$, which is about 1.5 standard deviations lower than the result reported here. A combination of our result with forthcoming CDF measurements will further improve the precision of the hadron collider measurements. This measurement and the new technique for tagging B_s^0 mesons will be useful in the studies of B_s^0 mixing and in B meson lifetime measurements in future runs of the Tevatron where an upgraded version of the CDF detector will be used.

IX. ACKNOWLEDGMENTS

We thank the Fermilab staff and the technical staff at the participating institutions for their essential contributions to this research. This work is supported by the U. S. Department of Energy and the National Science Foundation; the Natural Sciences and Engineering Research Council of Canada; the Istituto Nazionale di Fisica Nucleare of Italy; the Ministry of Education, Science and Culture of Japan; the National Science Council of the Republic of China; and the A. P. Sloan Foundation.

REFERENCES

[1] B. Andersson *et al.*, Phys. Rept. **97**, 31 (1983);
R. D. Field and R. P. Feynman, Nucl. Phys. **B136**, 1 (1978).

[2] J. Chrin, Z. Phys. C **36**, 163 (1987).

[3] C. Caso *et al.*, *The 1998 Review of Particle Physics*, The European Physical Journal **C3**, 1 (1998).

[4] D. Buskilic *et al.* (ALEPH Collaboration), Phys. Lett. **B369**, 151 (1996);
P. Abreu *et al.* (DELPHI Collaboration), Z. Phys. **C61**, 407 (1994);
P. Acton *et al.* (OPAL Collaboration), Phys. Lett. **B295**, 357 (1992).

[5] F. Abe *et al.* (CDF Collaboration), Phys. Rev. D **54**, 6596 (1996).

[6] F. Abe *et al.* (CDF Collaboration), Phys. Rev. D **59**, 032004 (1999).

[7] F. Abe *et al.* (CDF Collaboration), Nucl. Instrum. Methods Phys. Res. A **271**, 387 (1988);
F. Abe *et al.* (CDF Collaboration), Phys. Rev. D **52**, 4784 (1995);
P. Azzi *et al.*, Nucl. Instrum. Methods Phys. Res. A **360**, 137 (1995).

[8] F. Abe et al., Phys.Rev. D **57**, 5382 (1998).

[9] R. M. Barnett *et al.*, *The 1996 Review of Particle Physics*, Phys. Rev. D **54**, (1996) (see Section 28.6.4, page 166).

[10] P. Abreu *et al.* (DELPHI Collaboration), Z. Phys. **C68**, 375 (1997).

[11] F. Abe *et al.* (CDF Collaboration), Phys. Rev. D **58**, 112004 (1998).

[12] P. Nason, S. Dawson and R. K. Ellis, Nucl. Phys. **B327**, 49 (1989).

[13] A. D. Martin, W. J. Stirling and R. G. Roberts, Phys. Rev. D **47**, 867 (1993).

[14] C. Peterson, D. Schlatter, I. Schmitt and P. M. Zerwas, Phys. Rev. D **27**, 105 (1983).

[15] F. Paige and S. D. Protopescu, BNL report No. 38034, 1986 (unpublished).

[16] H.U. Bengtsson and T. Sjöstrand, Comput. Phys. Commun. **46**, 43 (1987).

[17] P. Avery, K. Read and G. Trahern, Cornell Internal Note CSN-212, 1985 (unpublished).

[18] F. Abe *et al.* (CDF Collaboration), Phys. Rev. D **58**, 072001 (1998).

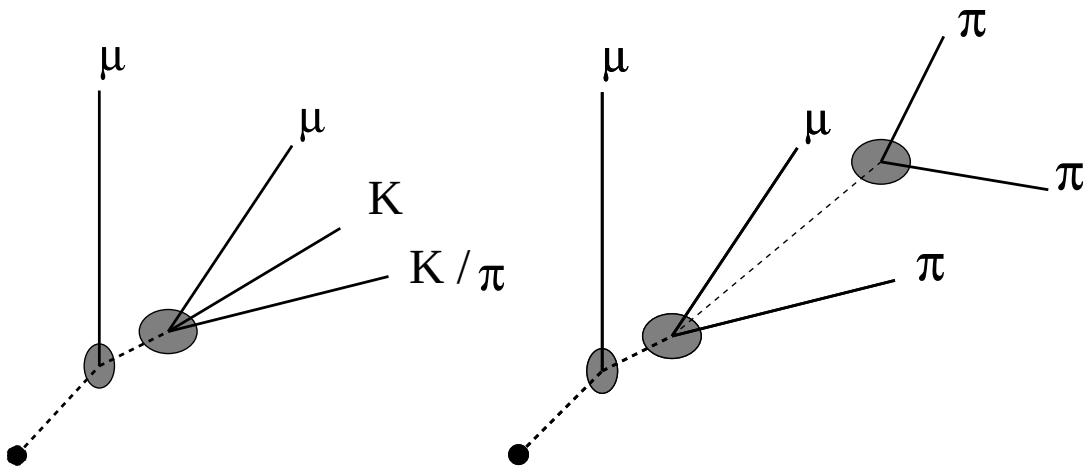

FIG. 1. Schematic of the vertex topology of ϕ/K^{*0} signal events (left) and K^{*+} signal events (right). The shaded areas represent the fitted secondary and tertiary decay vertices (not to scale).

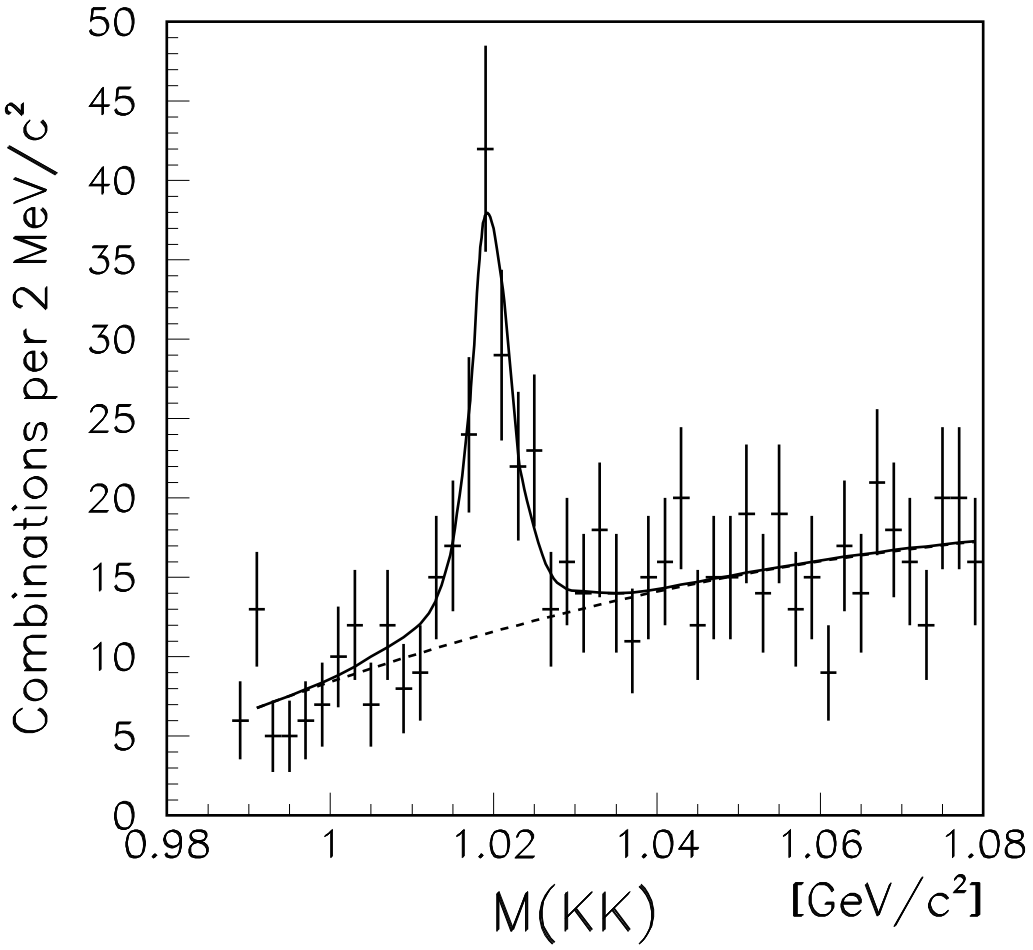

FIG. 2. The observed K^+K^- invariant mass distribution showing the ϕ meson signal in opposite sign dimuon events. The data are represented by crosses. The fit of the signal and background is shown with the solid line and the background component under the signal peak is indicated by the dashed line.

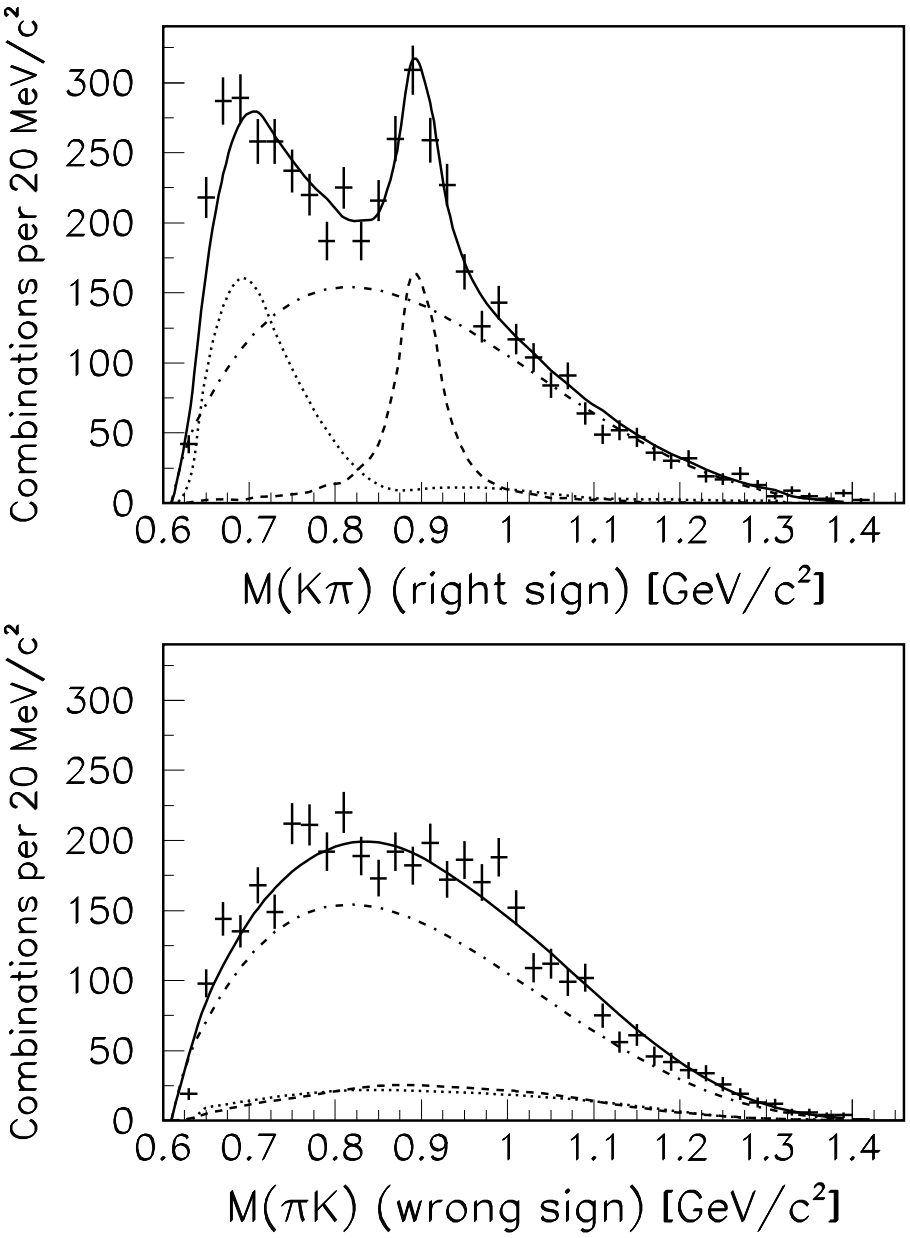

FIG. 3. The observed $K^+\pi^-$ invariant mass distributions showing the fit of the K^{*0} meson signal observed in opposite sign dimuon events. The top plot shows right-sign $K\pi$ combinations with respect to the muon from charm decay and the bottom plot shows the wrong sign distribution. Crosses represent the data and the solid line shows the fit result. Details of the fit components, shown with non-solid lines, are described in the text.

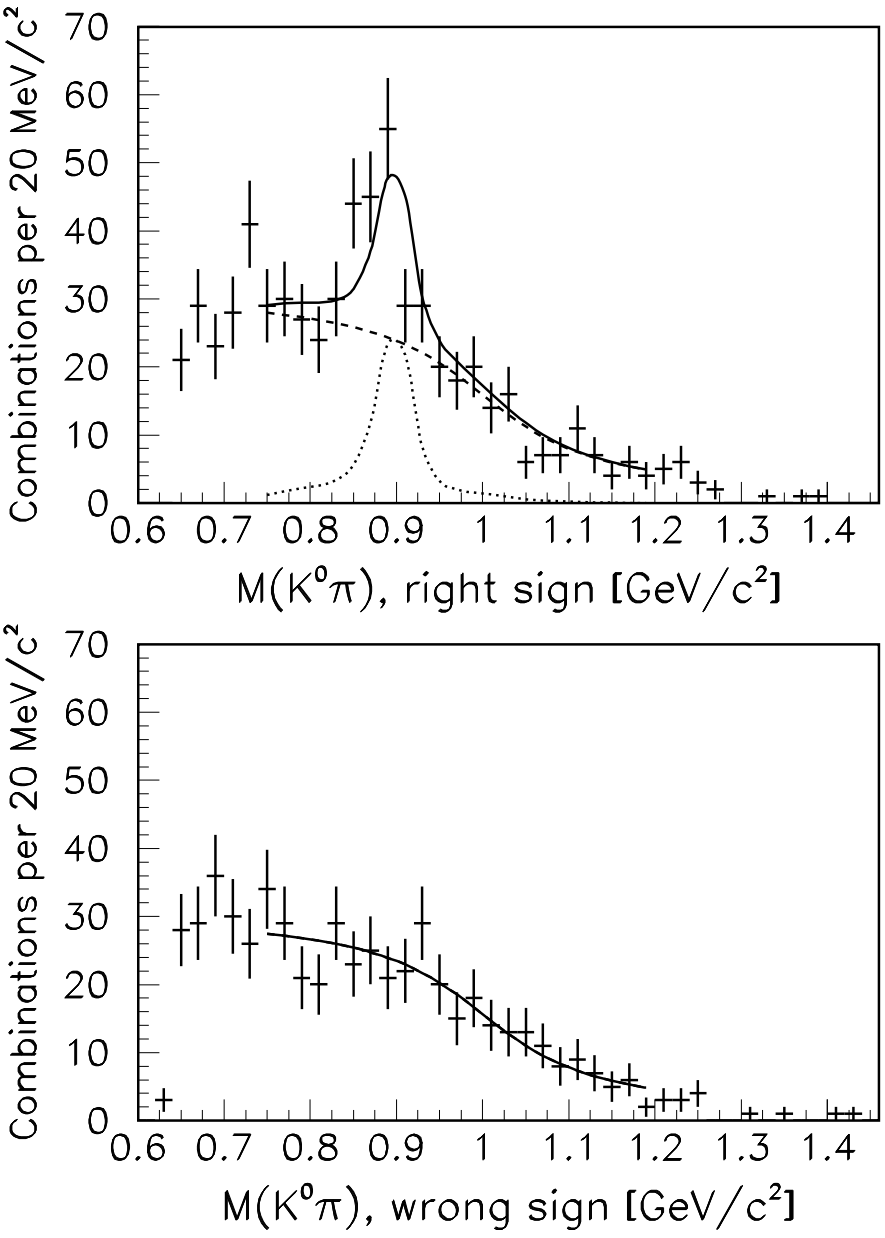

FIG. 4. Observed $K^0_S\pi^+$ invariant mass distributions showing the K^{*+} meson signal observed in opposite sign dimuon events. The top plot shows right-sign $K^0_S\pi^+$ combinations with respect to the muon from charm decay and the bottom plot shows the wrong sign distribution. Crosses represent the data. The solid line represents the fit result, the dotted line shows the K^{*+} signal and the dashed line shows the extrapolation of the combinatorial background under the signal peak.

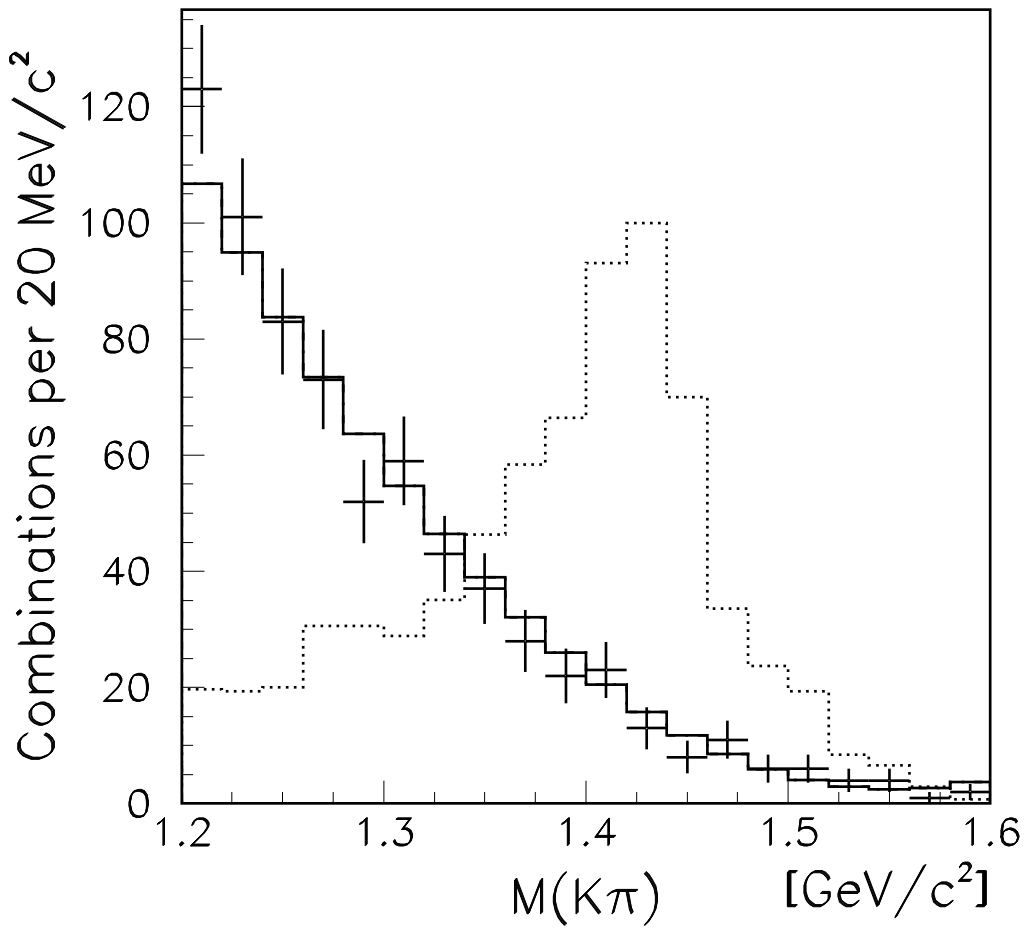

FIG. 5. Tail of the $M(K\pi)$ distribution observed in data (crosses) and the result of the fit (solid histogram). The dotted histogram shows the shape expected from $K_2^*(1430) \to K^+\pi^-$ decays. The normalisation of this histogram corresponds to the production of $K_2^*(1430)$ at thirty times the rate at which we set a limit.

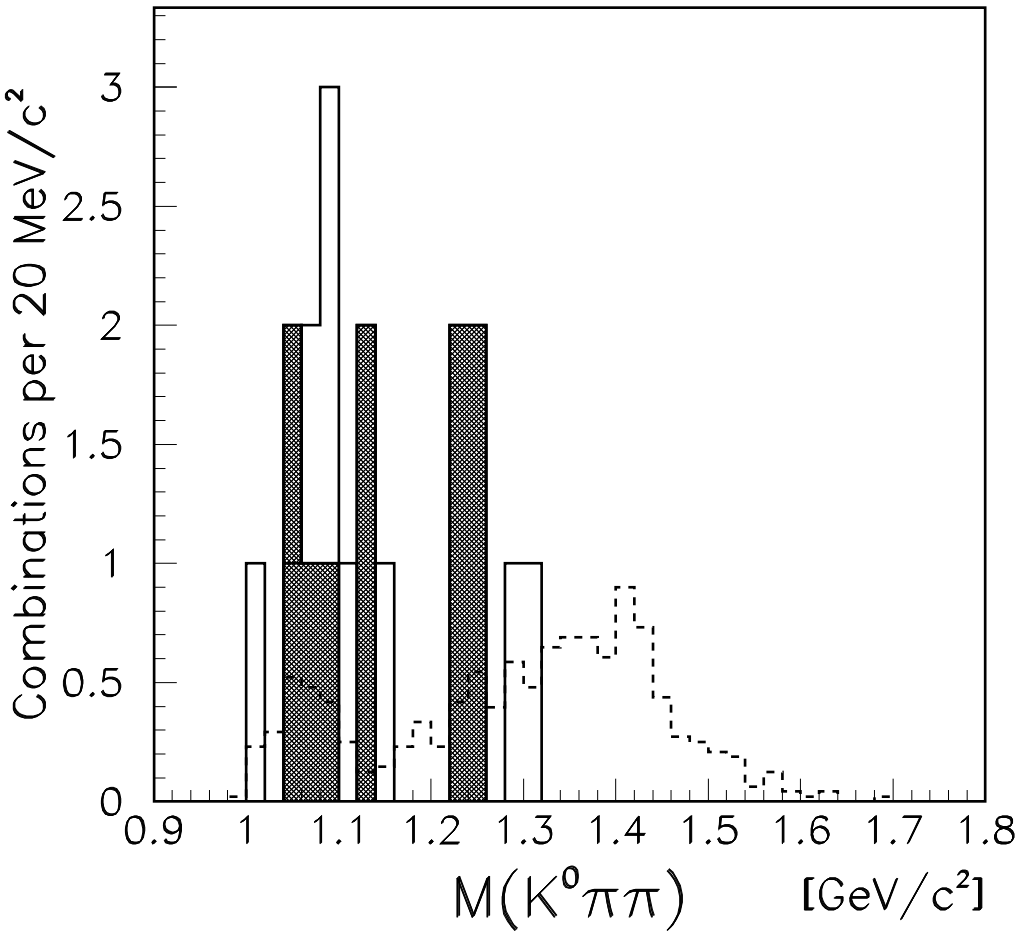

FIG. 6. The $M(K^0\pi\pi)$ distribution observed in data. The open solid histogram shows the distribution for right-sign (RS) combinations, while the hatched histogram shows the distribution for wrong-sign combinations. The open dashed histogram shows the signal expected in the RS distribution from $K_1^*(1410) \to K^0\pi\pi$ decays. The normalisation of this signal corresponds to the production of $K_1^*(1410)$ at the rate at which we set the 95% C.L. limit.

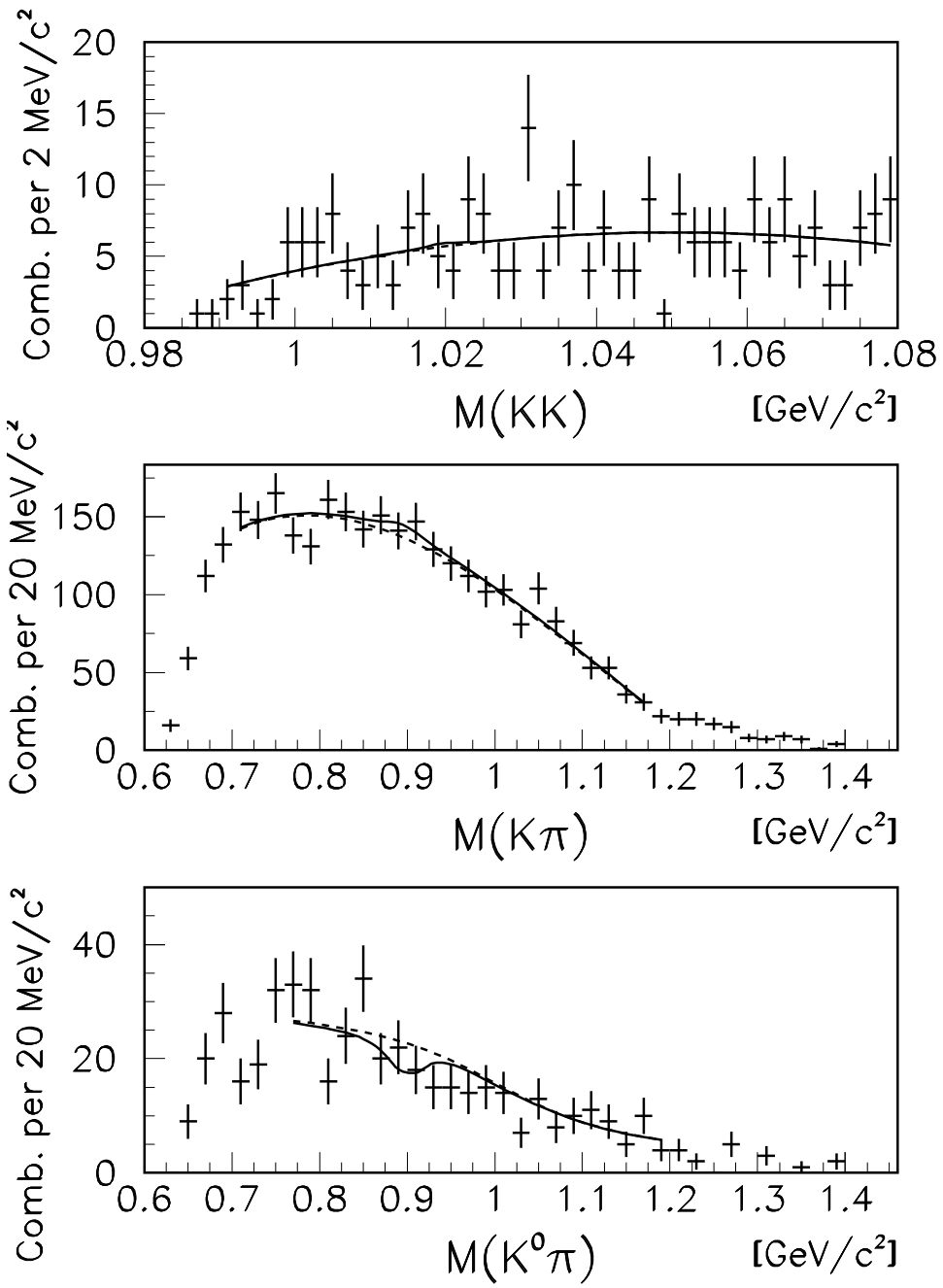

FIG. 7. Distributions of $M(K^+K^-)$ (top), $M(K^+\pi^-)$ (middle) and $M(K^0_S\pi^+)$ (bottom) observed in association with like-sign dimuon events. The data are represented by crosses. The fits to the ϕ, K^{*0} and K^{*+} meson signals, are shown with a solid line. The dashed lines indicate the shape of the background. The fits return values statistically consistent with zero.

TABLES

Signal	$\mu^+\mu^-$ signal	$\mu^\pm\mu^\pm$ signal	Background Correction
ϕ	103 ± 16	1 ± 15	13 ± 9
K^{*0}	683 ± 55	28 ± 41	75 ± 55
K^{*+}	94 ± 21	-20 ± 17	10 ± 8

TABLE I. Summary of the event yields. The fits to samples associated with like-sign dimuons provide a check for un-modeled backgrounds. The last column includes the background corrections described in section V for each of the signal channels.

Strange Meson Species	95% C.L. on β	84.1% C.L. on β (1σ)	Fraction in % of K^{*0} ($+1\sigma$)	Fraction in % of K^{*+} ($+1\sigma$)	Change in % on $f_s/(f_u + f_d)$
$K_1(1270)$	0.78	0.48	3.7 ± 1.5	9.3 ± 2.9	$+7.2 \pm 2.0$
$K_1^*(1410)$	0.60	0.34	9.8 ± 1.9	8.8 ± 1.8	$+10.6 \pm 1.6$
$K_2^*(1430)$	0.19	0.11	1.1 ± 0.1	1.5 ± 0.2	$+1.3 \pm 0.2$

TABLE II. Summary of limits on the heavy strange meson decays. We list the 95% C.L. limit on the ratio of the branching fraction into these states relative to that into $K^{*0}\mu\nu$ (see eqn. 8), the one sigma limit (used in the computation of the systematic uncertainties on this measurement), the one sigma correction (in %) to the event yields due to possible decays to these heavy strange mesons as well as the change (in %) induced on the final result if these channels are open at the level of the limit.

Meson	Lifetime Used (ps)
B^+	1.65 ± 0.04
B^0	1.56 ± 0.04
B_s^0	1.54 ± 0.07
D^+	1.057 ± 0.015
D^0	0.415 ± 0.004
D_s^+	0.467 ± 0.017

TABLE III. Meson lifetimes used as input to extract the final result on $f_s/(f_u + f_d)$.

Branching Fraction	Value Used
$\mathcal{B}(\phi \to K^+K^-)$	$(49.1 \pm 0.8)\%$
$\mathcal{B}(K^{*+} \to K^+\pi^-)$	2/3
$\mathcal{B}(K^{*0} \to K^0\pi^+)$	2/3
$\mathcal{B}(K^0 \to K_S^0)$	1/2
$\mathcal{B}(K_S^0 \to \pi^+\pi^-)$	$(68.61 \pm 0.28)\%$

TABLE IV. Meson branching fractions used as input to extract the final result on $f_s/(f_u + f_d)$.

Ratio of Branching Fraction	Values Used	Result
$\frac{\mathcal{B}(B^+\to D^0\mu^+\nu)}{\mathcal{B}(B^+\to\mu^+\nu X)}$	$\frac{(1.86\pm0.33)\%}{(10.3\pm0.9)\%}$	0.181 ± 0.036
$\frac{\mathcal{B}(B^0\to D^-\mu^+\nu)}{\mathcal{B}(B^0\to\mu^+\nu X)}$	$\frac{(2.00\pm0.25)\%}{(10.5\pm0.8)\%}$	0.190 ± 0.028
$\frac{\mathcal{B}(B^+\to D^{*0}\mu^+\nu)}{\mathcal{B}(B^+\to\mu^+\nu X)}$	$\frac{(5.3\pm0.8)\%}{(10.3\pm0.9)\%}$	0.514 ± 0.090
$\frac{\mathcal{B}(B^0\to D^{*-}\mu^+\nu)}{\mathcal{B}(B^0\to\mu^+\nu X)}$	$\frac{(4.60\pm0.27)\%}{(10.5\pm0.8)\%}$	0.438 ± 0.042

TABLE V. Ratios of branching fractions used to constrain f, f^* and f^{**} in the extraction of the final result on $f_s/(f_u + f_d)$.

Source of Uncertainty	contribution [%] of $f_s/(f_u+f_d)$
Statistical Uncertainty on $N(\phi)$	15.5
Statistical Uncertainty on $N(K^{*+})$	7.1
Statistical Uncertainty on $N(K^{*0})$	2.7
Total Statistical Uncertainty	17.3
Potential K^* from Heavy Strange Mesons	+10.7
Potential K^* from Λ_b	+2.0
Other K^{*0} Background	7.0
Other K^{*+} Background	1.0
ϕ Background	9.0
Total Background Uncertainty	$^{+15.6}_{-11.2}$
f,f^*,f^{**} Composition	5.9
$\tau(B_s)/\tau(B)$	5.2
$\tau(D_s)$	3.6
$\mathcal{B}(\phi \to K^+K^-)$	1.6
Tracking Efficiency for K^0_S daughters	1.4
$\tau(D^+)$	1.3
Trigger Acceptance	1.2
$\tau(D^0)$	0.1
$\mathcal{B}(K^0_S \to \pi^+\pi^-)$	0.1
Total Systematic Uncertainty	$^{+18.1}_{-14.4}$

TABLE VI. Statistical and systematic uncertainties as a fraction of the measured value, expressed in percent, on the measurement of $f_s/(f_u+f_d)$. Unless otherwise indicated the uncertainties are symmetric.